Research in Astronomy and Astrophysics, 23:045012 (12pp), 2023 April https://doi.org/10.1088/1674-4527/acc29c

Analytical Study of the Co-orbital Motion in the Circular Restricted Three-body Problem

Xinhe Shen[1,3], Tao Liu[1,4], and Xinhao Liao[1,2]
[1] Shanghai Astronomical Observatory, Chinese Academy of Sciences, Shanghai 200030, China; liutao@shao.ac.cn
[2] Key Laboratory of Planetary Sciences, Chinese Academy of Sciences, Shanghai 200030, China
[3] University of Chinese Academy of Sciences, Beijing 100049, China
[4] School of Physical Science and Technology, ShanghaiTech University, Shanghai 201210, China
Received 2022 December 14; revised 2023 February 4; accepted 2023 February 23; published 2023 March 30

Abstract

In the restricted three-body problem (RTBP), if a small body and a planet stably orbit around a central star with almost exactly the same semimajor axis, and thus almost the same mean motion, this phenomenon is called the co-orbital motion, or equivalently, the 1:1 mean motion resonance. The classical expansion of the disturbing function is divergent when the semimajor axis ratio of the small body to the planet is close to unity. Thus, most of the previous studies on the co-orbital dynamics were carried out through numerical integrations or semi-analytical approaches. In this work, we construct an analytical averaged model for the co-orbital motion in the framework of the circular RTBP. This model is valid in the entire coorbital region except in the vicinity of the collision singularity. The results of the analytical averaged model are in good agreement with the numerical averaged model even for moderate eccentricities and inclinations. The analytical model can reproduce the tadpole, horseshoe and quasi-satellite orbits common in the planar problem. Furthermore, the asymmetry of 1:1 resonance and the compound orbits (Icarus 137:293–314) in the general spatial problem can also be obtained from the analytical model.

Key words: celestial mechanics – methods: analytical – minor planets – asteroids: general

1. Introduction

The co-orbital motion or 1:1 mean motion resonance is one of the most interesting topics of the three-body problem and has been extensively studied for more than 100 yr. The history of the co-orbital motion began with the work of Euler and Lagrange in the 18th century. In 1767, Euler found that the general three-body problem has three special solutions in which the three masses are collinear at each instant. In 1772, Lagrange found a second kind of special solutions to the general three-body problem in which the three masses form an equilateral triangle at each instant. In the circular restricted case, these special solutions correspond to the well-known Lagrangian equilibrium points: the collinear points L_1, L_2, L_3; the triangular points L_4 and L_5. The Lagrangian points L_4 and L_5 are linearly stable to small displacements when $\epsilon < 0.0385$, where $\epsilon = m_2/(m_1 + m_2)$ is the mass ratio of the system (Gascheau 1843). This implies that a small body can remain near L_4 or L_5 and thus stably share the same orbit with a planet. Such a small body is called a Trojan. The first Trojan asteroid, 588 Achilles, which is librating around Jupiter's L_4, was discovered by Max Wolf of the Heidelberg Observatory in 1906.

The 1:1 mean motion resonance manifests itself in a variety of modes of motion. The different modes of motion can be distinguished according to the librational behavior of the resonant angle, $\tilde{l} = \lambda - \lambda'$, where λ and λ' are the mean longitudes of the small body and the planet respectively. There are three elementary modes of co-orbital motion: (i) tadpole (T) or Trojan orbits, where $\tilde{l}$ librates around L_4 or L_5; (ii) horseshoe (HS) orbits, where $\tilde{l}$ librates around L_3 with an amplitude larger than 180° encompassing L_4 and L_5; (iii) quasi-satellite (QS) orbits, associated with a libration of $\tilde{l}$ around 0°. It is important to point out that the Lagrangian points L_4 and L_5 (i.e., the libration centers of the tadpole motion) are exactly located at $\tilde{l} = \pm 60°$ only when the small body's orbit is circular and planar; for eccentric and inclined orbits of the small body the effective Lagrangian points L_4 and L_5 will be displaced appreciably from $\tilde{l} = \pm 60°$ (Namouni & Murray 2000). Apart from these three elementary co-orbital orbit families, in the spatial case the quasi-satellite orbits can merge with horseshoe or tadpole orbits to form the stable compound orbits, H–QS, T–QS and T–QS-T (Namouni 1999; Namouni et al. 1999; Christou 2000). The compound T–QS orbits, which are also called the large-amplitude tadpole orbits, librate around 0° with amplitudes less than 180° and encompassing L_4 or L_5. In the compound T–QS-T mode, $\tilde{l}$ librates around 0° with an amplitude larger than 180° encompassing L_4 and L_5. A compound H–QS orbit corresponds to an asymmetric horseshoe-like libration around L_3 with a narrow opening ahead or behind the quasi-satellite domain.

A classical example of the tadpole motion is the Jovian Trojan population containing several thousand members. Trojan asteroids have also been found for Venus, Earth, Uranus and Neptune (see Greenstreet et al. 2020, and references therein). The horseshoe motion was first observed in the Saturnian satellite pair Janus-Epimetheus during Voyager 1 flyby of Saturn in 1980 (Synnott et al. 1981). There are several confirmed horseshoe objects coorbiting with the Earth (Kaplan & Cengiz 2020). The first known object following a quasi-satellite path was asteroid 2002 VE_{68} which is a companion to Venus (Mikkola et al. 2004). The Earth and Jupiter host the largest known number of quasi-satellites with at least eight in the solar system; while Venus, Saturn, Neptune and dwarf planet Ceres have one each (de la Fuente Marcos & de la Fuente Marcos 2016). Asteroid 3753 Cruithne, a co-orbital of the Earth, is recognized to be moving in a compound H–QS orbit (Wiegert et al. 1998; Namouni 1999). Another example of a H–QS orbit is Venus' co-orbital 2001 CK_{32} (Brasser et al. 2004). A probable candidate for the compound T–QS-T orbit is asteroid 2013 LX_{28}, locked in 1:1 resonance with the Earth (de la Fuente Marcos & de la Fuente Marcos 2014).

Dermott & Murray (1981a, 1981b) studied the fundamental properties of quasi-circular tadpole and horseshoe orbits by means of the Jacobi integral and numerical integration; for the first time they gave a detailed description of the horseshoe motion of Janus-Epimetheus system with comparable masses. Yoder et al. (1983) derived an analytic approximation to the tadpole and horseshoe motions, which includes the second-order correction to the 1:1 resonance caused by eccentricities and inclinations. A Hamiltonian secular theory for Trojan-type motion was constructed in the framework of the elliptic restricted three-body problem (RTBP) by Morais (1999, 2001). Although these analytical theories presented in Yoder et al. (1983) and Morais (1999, 2001) are enough to describe the tadpole and horseshoe motions, they break down when $\tilde{l} = 0°$ and thus are not applicable to the quasi-satellite motion. Namouni (1999) investigated the co-orbital dynamics analytically using the Hill's three-body problem and showed that in the spatial case recurrent transitions between horseshoe, tadpole and quasi-satellite orbits are possible. However, the Hill's three-body problem is accurate only for sufficiently small mass ratios and small eccentricities and inclinations. Moreover, the asymmetry of the spatial 1:1 resonance with respect to $\tilde{l} = 0°$, resulting in the stable and asymmetric merger of horseshoe or tadpole with quasi-satellite orbits, is absent in the Hill's problem. Thus, he reverted to the numerical integrations of the full equations of motion and then found new types of co-orbital orbits referred as "compound orbits" (see also Namouni et al. 1999). Later, following Schubarts numerical averaging of the Hamiltonian over the fast variable, Nesvorný et al. (2002) studied the global structure of the phase space of 1:1 resonance, and they replicated these new compound orbits in their semi-analytical model. Such numerical averaging methods have been used in many researches on the co-orbital motion (e.g., Beaugé & Roig 2001; Giuppone et al. 2010; Sidorenko et al. 2014; Pousse & Robutel 2017; Qi & de Ruiter 2020). In particular, Robutel & Pousse (2013) as well as Giuppone & Leiva (2016) derived an analytical Hamiltonian formalism adapted to the study of the dynamics of two planets in 1:1 resonance. However, since in their works the planetary Hamiltonian is literally expanded in powers of eccentricity and inclination with respect to zero eccentricity and zero inclination (i.e., the circular and coplanar orbit), the expansion of the planetary Hamiltonian is inherently singular at $\alpha = 1$ and $\tilde{l} = 0°$ (where α is the semimajor axis ratio of the two planets). This will give rise to incorrect phase space structures of 1:1 resonance for large/moderate eccentricities and inclinations.

In this paper, we develop an analytical averaged model which is valid in the entire regular co-orbital region and is applicable to both the planar and spatial problems. Using the analytical model we can recover all known co-orbital orbit families, including the tadpole, horseshoe, quasi-satellite, and compound orbits. The analytical averaged model is in good agreement with the numerical averaged model even for moderate eccentricities (<0.3) and inclinations (<30°). The paper is organized as follows. In Section 2, we introduce the analytical averaged model for the co-orbital motion of the circular RTBP. In Section 3, we study the phase space structure of the co-orbital dynamics using the analytical model. A comparison of the analytical averaged model with the numerical averaged model is presented in Section 4. Finally, we summarize the paper in Section 5.

2. The Analytical Model

We consider the circular restricted three-body problem consisting of a small body of negligible mass, a central star of mass $M_\star$ and a planet of mass m' orbiting the star in a circular orbit. We shall use the standard notations a, e, i, ω, Ω, M and f for the semimajor axis, eccentricity, inclination, argument of perihelion, longitude of ascending node, mean anomaly, and true anomaly of the small body. We further define $\lambda = M + \omega + \Omega$ and $\theta = f + \omega + \Omega$ to be the mean longitude and true longitude of the small body, respectively. Similar primed quantities refer to the planet.

The Hamiltonian of the circular restricted three-body problem is

$$F = -\frac{\mu}{2a} - R, \tag{1}$$

where $\mu = GM_\star$ and G is the gravitational constant. R is the disturbing function given by

$$R = Gm'\left(\frac{1}{\Delta} - \frac{r}{a'^2}\cos\psi\right), \tag{2}$$

with

$$\Delta^2 = r^2 + a'^2 - 2ra'\cos\psi, \tag{3}$$

where Δ is the distance of the small body from the planet; $r = a(1-e^2)/(1+e\cos f)$ is the orbital radius of the small body; and ψ is the angle between the position vectors of the small body and the planet, given by

$$\cos\psi = \cos^2\frac{i}{2}\cos(\theta - M') + \sin^2\frac{i}{2}\cos(\theta + M' - 2\Omega). \tag{4}$$

The first term of the disturbing function R is called the direct perturbation term which accounts for the gravitational interaction between the planet and the small body. The second term is called the indirect term which arises from the choice of the non-inertial heliocentric frame.

It is convenient to describe the 1:1 mean motion resonance in the circular RTBP using the following canonical conjugate variables:

$$\begin{aligned} \widetilde{L} &= \sqrt{\mu a}, & \tilde{l} &= M + \omega + \Omega - M' \\ \widetilde{G} &= \sqrt{\mu a(1-e^2)} - \sqrt{\mu a}, & \tilde{g} &= \omega \\ \widetilde{H} &= \sqrt{\mu a(1-e^2)}\cos i - \sqrt{\mu a}, & \tilde{h} &= \Omega. \end{aligned} \tag{5}$$

Using the definition $\tilde{l} = M + \omega + \Omega - M'$, $\cos\psi$ can be written as

$$\cos\psi = \cos^2\frac{i}{2}\cos(\tilde{l} + f - M) + \sin^2\frac{i}{2}\cos(\tilde{l} - 2\omega - f - M). \tag{6}$$

The Hamiltonian for the circular RTBP expressed in terms of canonical variables in Equation (5) reads

$$F = -\frac{\mu^2}{2\widetilde{L}^2} - n'\widetilde{L} - R(\widetilde{L}, \widetilde{G}, \widetilde{H}, \tilde{l}, \tilde{g}, M), \tag{7}$$

where n' is the mean motion of the planet. Note that the Hamiltonian in Equation (7) is independent of $\tilde{h}$, hence its conjugate momentum $\widetilde{H}$ remain constant.

In the 1:1 resonance, the resonant angle $\tilde{l}$ varies slowly with time compared to the mean motions of the small body and the planet. In fact, there are three dynamical timescales which have a hierarchical separation. The shortest timescale, associated with the orbital motions of the small body and the planet, is of order $\mathcal{O}(T)$ (where T is the orbital period of the small body). The intermediate timescale associated with the libration of $\tilde{l}$ is of order $\mathcal{O}(T/\sqrt{\epsilon})$. The longest timescale associated with the secular evolution of ω and Ω is of order $\mathcal{O}(T/\epsilon)$ (Wisdom 1985; Leleu et al. 2018). This separation ensures that the short-period perturbations arising from the orbital motions do not affect the evolution of resonant and secular phases because their contributions tend to zero on average. Thus, the short-period terms containing M can be eliminated from the Hamiltonian in Equation (7) to simplify the problem, which is achieved by averaging the Hamiltonian over M.

The averaged Hamiltonian over the mean anomaly M is given by

$$\overline{F} = \frac{1}{2\pi}\int_0^{2\pi} F\, \mathrm{d}M. \tag{8}$$

The averaged Hamiltonian does not depend explicitly on time and therefore is autonomous. In order to find an analytical expression for the averaged Hamiltonian, first we expand the Hamiltonian in Equation (7) to second order in e and $\sin(i/2)$. Then, averaging the expansion of the Hamiltonian (7) with respect to M, we obtain the analytical averaged Hamiltonian

$$\overline{F} = -\frac{\mu^2}{2\widetilde{L}^2} - n'\widetilde{L} - Gm'\left[\overline{\left(\frac{1}{\Delta}\right)} - \frac{\overline{r\cos\psi}}{a'^2}\right], \tag{9}$$

where

$$\begin{aligned} \overline{\left(\frac{1}{\Delta}\right)} = \overline{\left(\frac{1}{\Delta_0}\right)} &+ e^2\sin^2\frac{i}{2}\frac{aa'}{\Delta_{00}^3} \\ &\times\left\{\left[\frac{1}{8} - \frac{15}{8}\frac{a^2}{\Delta_{00}^2} + \frac{15}{8}\frac{a^4}{\Delta_{00}^4} - \frac{45}{16}\frac{a^2a'^2}{\Delta_{00}^4}\cos^4\frac{i}{2}\right]\right. \\ &\times\cos(\tilde{l} - 2\omega) \\ &+\left[\frac{57}{16}\frac{aa'}{\Delta_{00}^2} - \frac{45}{8}\frac{a^3a'}{\Delta_{00}^4}\right]\cos^2\frac{i}{2}\cos 2\omega \\ &+\left[-\frac{9}{16}\frac{aa'}{\Delta_{00}^2} + \frac{15}{8}\frac{a^3a'}{\Delta_{00}^4}\right]\cos^2\frac{i}{2}\cos(2\tilde{l} - 2\omega) \\ &+\frac{135}{32}\frac{a^2a'^2}{\Delta_{00}^4}\cos^4\frac{i}{2}\cos(\tilde{l} + 2\omega) \\ &\left.+\frac{15}{32}\frac{a^2a'^2}{\Delta_{00}^4}\cos^4\frac{i}{2}\cos(3\tilde{l} - 2\omega)\right\}, \end{aligned} \tag{10}$$

$$\overline{r\cos\psi} = a\left[\cos^2\frac{i}{2}\left(1 - \frac{1}{2}e^2\right)\cos\tilde{l} + \frac{1}{8}e^2\sin^2\frac{i}{2}\cos(\tilde{l} - 2\omega)\right], \tag{11}$$

with

$$\overline{\left(\frac{1}{\Delta_0}\right)} = \frac{1}{2}\left[\frac{1}{\sqrt{\Delta_{00}^2 - \Delta_{01}}} + \frac{1}{\sqrt{\Delta_{00}^2 + \Delta_{01}}}\right], \tag{12}$$

and

$$\Delta_{00}^2 = a^2\left(1 + \frac{3}{2}e^2\right) + a'^2 - 2aa'\left(1 - \frac{1}{2}e^2\right)\cos^2\frac{i}{2}\cos\tilde{l}, \tag{13}$$

$$\Delta_{01}^2 = e^2\left(2a^4 + 5a^2a'^2\cos^4\frac{i}{2}\right) - 4e^2a^3a'\cos^2\frac{i}{2}\cos\tilde{l} - 3e^2a^2a'^2\cos^4\frac{i}{2}\cos 2\tilde{l}. \quad (14)$$

A detailed derivation of the Hamiltonian (9) is presented in the Appendix. The averaged Hamiltonian can also be obtained by numerically integrating Equation (8). This numerical averaging treatment was first introduced by Schubart (1964) as a semi-analytical approach to the mean motion resonance. In this paper, we will call the numerical integration of the averaged Hamiltonian (8) "the numerical averaged model" and we call the Hamiltonian (9) "the analytical averaged model".

3. Phase Space of 1:1 Mean Motion Resonance

In this section, we explore the phase space of the 1:1 mean motion resonance using the analytical averaged model. For the sake of simplicity, we will chose a system of units such that $m = 1$, $a' = 1$ and $G = 1$. Without loss of generality we set $m' = 10^{-3}$ (a Jupiter-mass planet).

3.1. The Planar Case

In the planar ($i = 0°$) case, the Hamiltonian does not depend on ω and thus $\widetilde{G}$ is a constant. At this stage, the Hamiltonian has been reduced to one degree of freedom related to the conjugate pair $(\widetilde{L}, \tilde{l})$, and is only parameterized by $\widetilde{G}$. The Hamiltonian is now integrable. Given values of $\widetilde{G}$, we can obtain the phase-space trajectories in the $(a, \tilde{l})$ plane (topologically equivalent to the $(\widetilde{L}, \tilde{l})$ plane) by computing the level curves of the analytical averaged Hamiltonian in Equation (9). The value of $\widetilde{G}$ is determined by a pair of reference elements a_0 and e_0, that is, $\widetilde{G} = \sqrt{a_0(1 - e_0^2)} - \sqrt{a_0}$. Throughout this work we assume $a_0 = 1$, then e_0 is the value of eccentricity at the Lagrangian point L_4 (or L_5). The greater e_0 means more eccentric orbits of the small body.

In Figure 1, we show the phase portraits of the planar 1:1 resonance obtained in the analytical averaged model for $e_0 = 0$, 0.1, 0.2 and 0.3. For $e_0 = 0$ (see Figure 1(a)), the phase space morphology is similar to the classical zero-velocity curves of the circular restricted three-body problem; the system has five equilibrium points, corresponding to the five Lagrangian points. L_4 and L_5 are exactly located at $\tilde{l} = 60°$and $-60°$ respectively, and L_3 at $\tilde{l} = 180°$. In Figure 1(a) there are tadpole trajectories enclosing L_4 (or L_5) and horseshoe trajectories enclosing L_3, L_4 and L_5. For $e_0 = 0.1$, 0.2 and 0.3 (see Figures 1(b)–(d)), there is an equilibrium point at $\tilde{l} = 0°$, and the quasi-satellite trajectories librating around the equilibrium point appear in the phase space. Moreover, as e_0 increases the size of the quasi-satellite domain increases, which is consistent with the previous works (see, e.g., Nesvorný et al. 2002; Pousse & Robutel 2017). It is clear in Figure 1 that the structure of the phase space for the planar case is symmetrical with respect to $\tilde{l} = 0°$.

When $\Delta = 0$ the Hamiltonian (1) as well as (8) becomes infinite, that is, the Hamiltonian (1)/(8) has a singularity that corresponds to the collision between the small body and the planet. However, the collision singularity has been removed from the analytical averaged Hamiltonian in Equation (9) (except for the case of $e = 0$ and $i = 0°$) due to the expanding manipulation of the analytical Hamiltonian. Hence there are no collision curves in Figures 1(b)–(d). This is a difference difference between the analytical averaged model and the numerical averaged model. In fact, the averaging method is not applicable to the dynamics in the neighborhood of the collision singularity (i.e., the Hill region of the planet) because the hierarchical separation between the timescales of the different variables breaks down in the Hill region (Robutel et al. 2016; Pousse & Robutel 2017). Thus, the averaged model, whether analytical or numerical, cannot give real phase trajectories in the vicinity of the collision curves. This is an inherent drawback of the averaged method.

We can write $a = 1 + \Delta a$ as the small body is coorbiting with the planet. Moreover, in our case: $m' \ll \Delta a \ll 1$. Thus, according to Equation (9) the phase trajectories can be approximately described by Wajer (2009)

$$(\Delta a)^2 = \frac{8m'}{3}(C - R^*(a, \tilde{l})), \quad (15)$$

where $R^* = \overline{R}/m'$ and C is a constant that determines the type of the trajectory. The time evolution of the semimajor axis, da/dt, is given by

$$\frac{da}{dt} = 2Lm'^2\frac{\partial R^*}{\partial \tilde{l}}. \quad (16)$$

Hence the shape of R^* is crucial because the extrema of R^* define the location of stable and unstable equilibrium points. The minima of R^* define the stable equilibrium points, i.e., libration centers around which there are the librating trajectories; while the maxima define the unstable equilibrium points (saddles) (Gallardo 2006). We define

$$S(\tilde{l}) \triangleq R^*(1, \tilde{l}). \quad (17)$$

$S(\tilde{l})$ corresponds to a curve formed by the intersection of the surface $R^*(a, \tilde{l})$ with the plane $a = 1$. The curve gives the location of the equilibrium points in the resonant angle $\tilde{l}$. The behavior of S would help us to understand better the nature of the different trajectories in 1:1 resonance.

Figure 2 shows two examples of the behavior of S as a function of $\tilde{l}$ for $e_0 = 0$ and 0.3. For $e_0 = 0$, S has two minima at $\tilde{l} = \pm 60°$ and a local maximum at $\tilde{l} = 180°$, which correspond to the stable Lagrangian points L_4 and L_5 and the unstable L_3 (see left panel of Figure 2). The values of S at L_3, L_4 and L_5 are denoted by S_{L_3}, S_{L_4} and S_{L_5}, respectively. In the

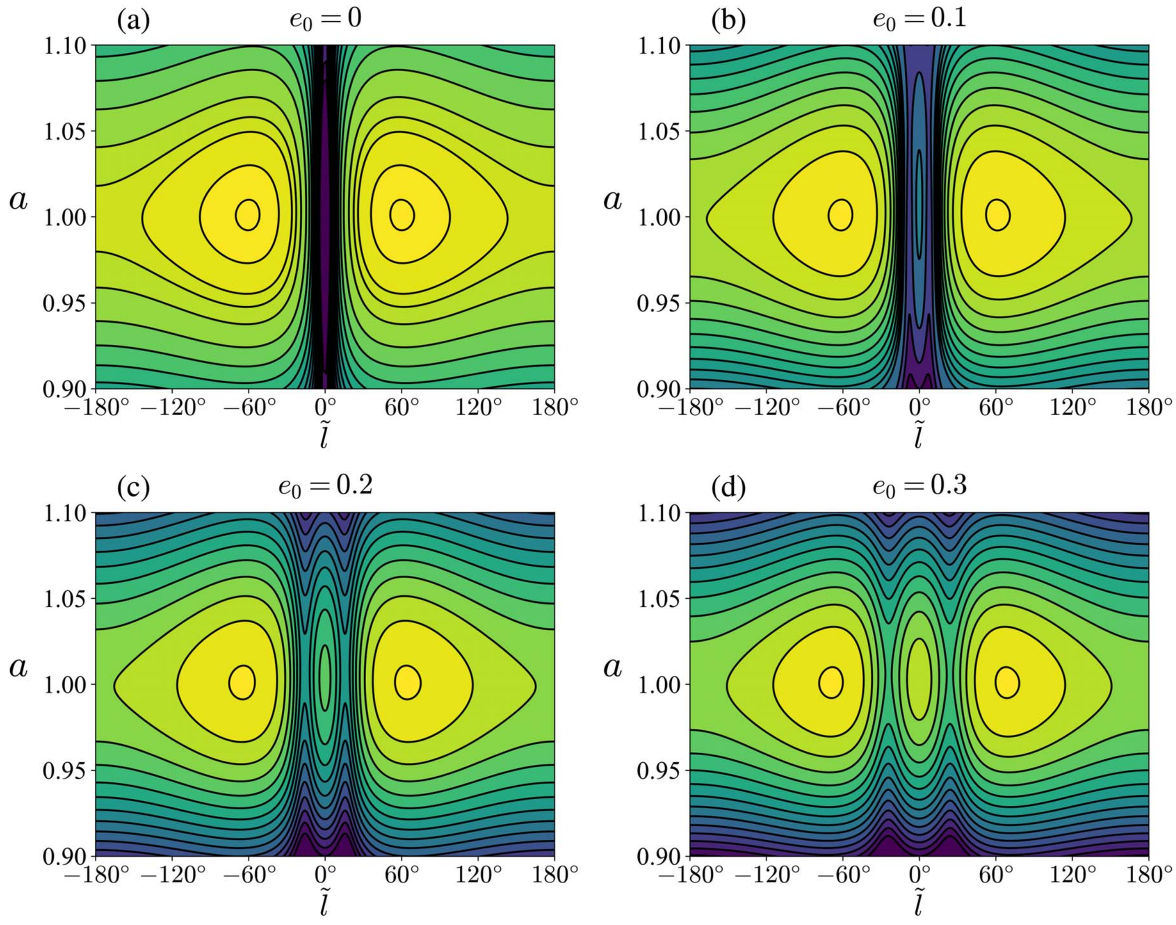

Figure 1. The phase portraits of the planar 1:1 resonance in the $(a, \tilde{l})$ plane for $e_0 = 0$, 0.1, 0.2 and 0.3. The curves represent the level curves of the Hamiltonian (9), and the background color maps represent the variation of the value of the Hamiltonian (9).

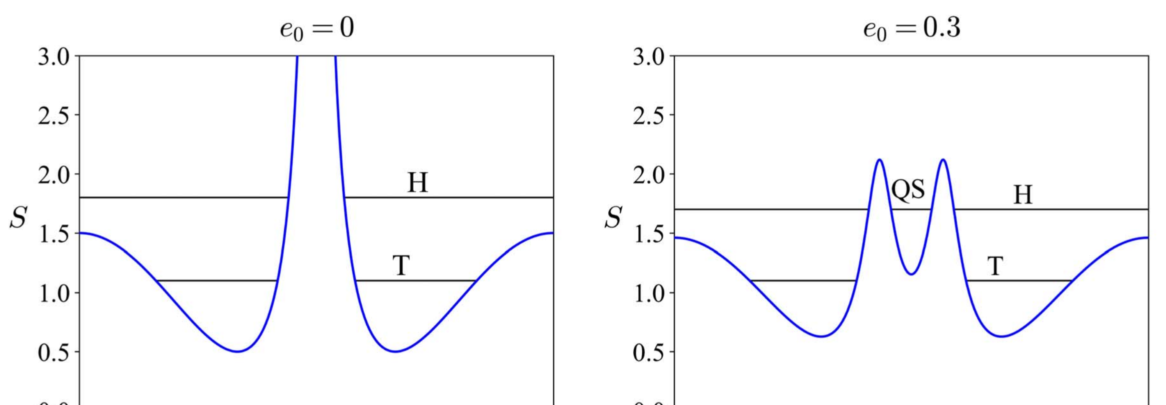

Figure 2. $S(\tilde{l})$ as a function of $\tilde{l}$ for $e_0 = 0$ (left) and 0.3 (right) in the planar case. T, H and QS denote tadpole, horseshoe and quasi-satellite orbits, respectively. The black horizontal lines correspond to the constant values of C.

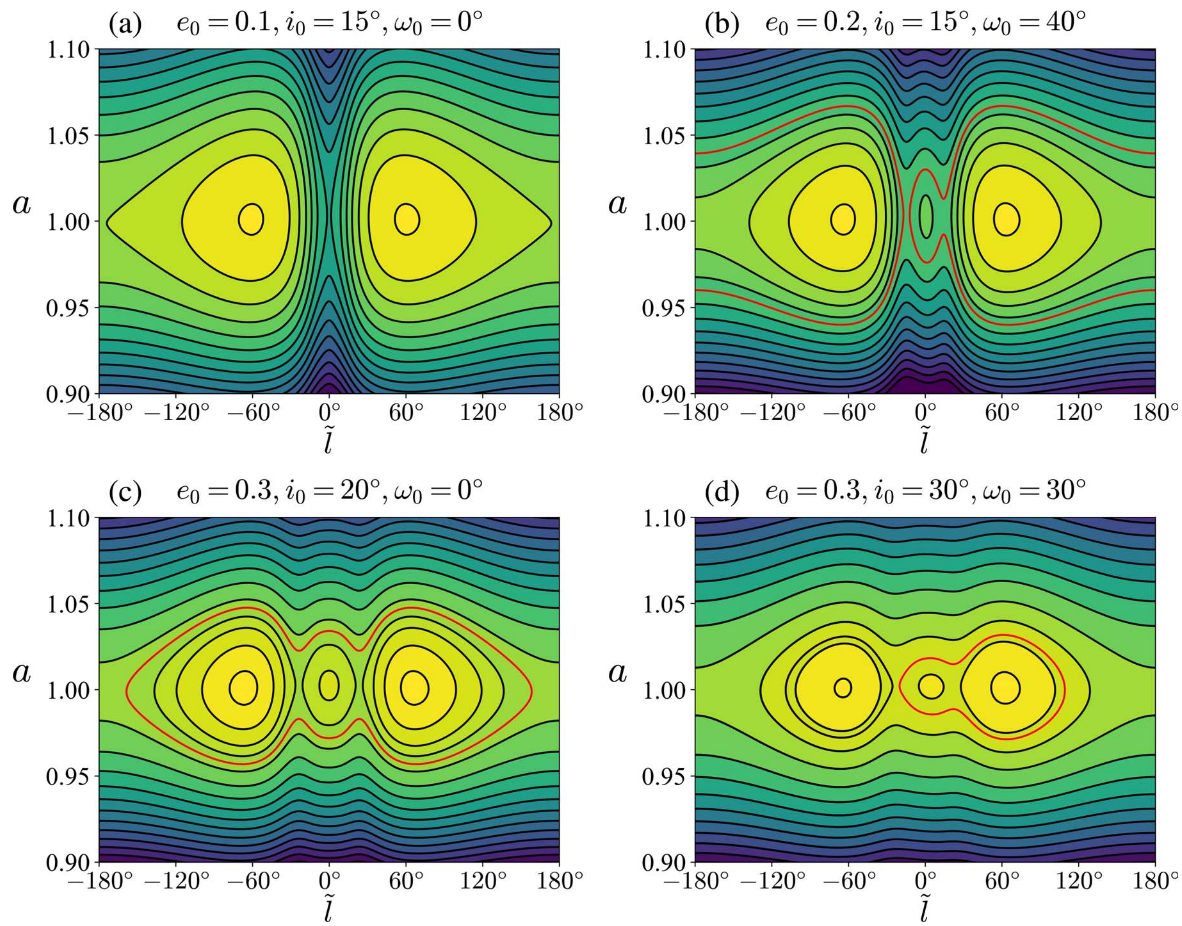

Figure 3. The phase portraits of the spatial 1:1 resonance in the $(a, \tilde{l})$ plane for a selection of values of e_0, i_0 and ω_0. The curves are the level curves of the Hamiltonian (9), and the background color maps represent the variation of the value of the Hamiltonian (9). The red lines in (b)–(d) denote the compound H–QS, T–QS-T and T–QS orbits, respectively.

planar case we have $S_{L_4} = S_{L_5}$. Orbits with the values of C larger than S_{L_4} and smaller than S_{L_3} are tadpole; orbits with $C > S_{L_3}$ are horseshoe. For $e_0 = 0.3$ (left panel of Figure 2), two sharp peaks (local maxima) of S appear near $\tilde{l} = 0$. The value of the peak to the right of $\tilde{l} = 0$ is denoted by S_+, and to the left S_-. In the planar case $S_+ = S_-$. Moreover, there is also a local minimum at $\tilde{l} = 0$ denoted as S_0, which corresponds to the libration center of the quasi-satellite trajectories (see Figure 1(d)). Orbits with $S_0 < C < S_+$ are quasi-satellite. We also see that for $e_0 = 0.3$ the Lagrangian points L_4 and L_5 are displaced from $\tilde{l} = \pm 60°$ toward $\pm 180°$.

3.2. The Spatial Case

In the spatial case, the Hamiltonian (9) is not independent of ω, hence $\widetilde{G}$ is not a constant. However, since ω and $\widetilde{G}$ vary on a timescale much longer than the period of 1:1 resonance, we may assume ω, $\widetilde{G}$ to be fixed parameters (adiabatic approximation, see Beaugé & Roig 2001). As a result, the problem has been reduced to a one degree of freedom system, and the Hamiltonian (9) is now parameterized by ω, $\widetilde{G}$ and $\widetilde{H}$. We choose a set of reference elements a_0, e_0, i_0 and ω_0 which determine the values of $\widetilde{G}$ and $\widetilde{H}$, that is, $\widetilde{G} = \sqrt{(1 - e_0^2)} - 1$ and $\widetilde{H} = \sqrt{(1 - e_0^2)}\cos i_0 - 1$ (note that we have assumed $a_0 = 1$).

Figure 3 shows the phase portraits of the spatial 1:1 resonance obtained in the analytical averaged model for a selection of reference elements. In Figure 3(a) the quasi-satellite domain disappear and there are only tadpole and horseshoe orbits. In this case the minimal angular separations of the horseshoe orbits could reach very small value ($\sim 0°$). However, these horseshoe orbits might be unstable because the equilibrium point at $\tilde{l} = 0$ is a saddle (Figure 4(a)), near which chaos occur. In Figure 3(b), the compound H–QS orbits appear as a result of the merger of horseshoe orbits with quasi satellite orbits. The H–QS orbit has a horseshoe-like trajectory but enclosing the quasi-satellite domain and has a narrow opening

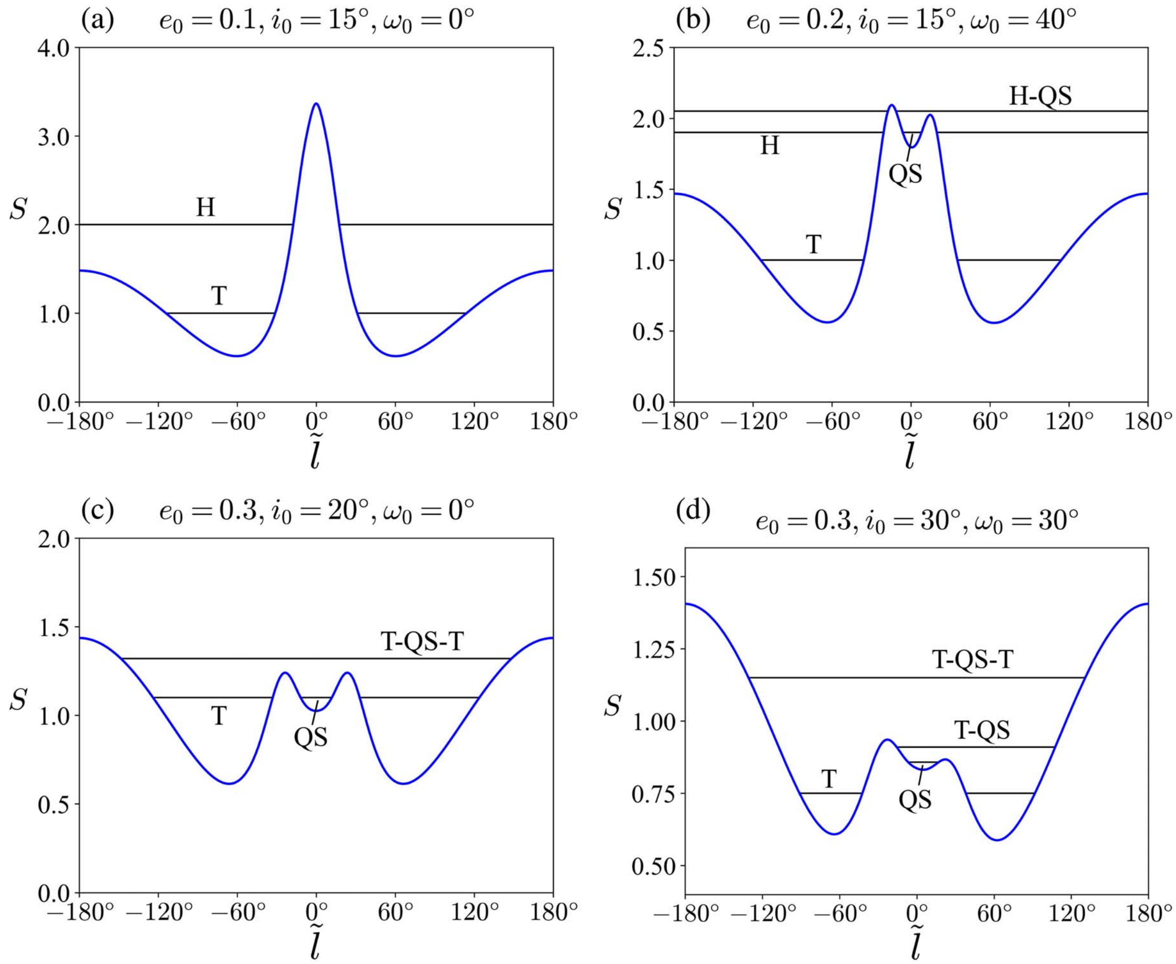

Figure 4. $S(\tilde{l})$ as a function of $\tilde{l}$ for a selection of reference elements same as in Figure 3.

to the left of $\tilde{l} = 0°$ (see the red line in Figure 3(b)). In Figures 3(c) and (d), there are compound T–QS-T orbits formed by the merger of the quasi-satellite orbits with the L_4 and L_5 tadpole orbits. The T–QS-T orbit makes the transfer of the small body from L_4 tadpole region to L_5 tadpole region possible, and vice versa. In Figure 3(d), we show an example of the compound T–QS orbit which is formed by the merger of the quasi-satellite and tadpole orbits. From the Hamiltonian in Equation (9) we note that, in the spatial case, only when $\cos 2\omega = 0$ and ± 1 the following relationship holds

$$\overline{F}(\tilde{l}, \widetilde{L}, \widetilde{G}, \widetilde{H}, \omega) = \overline{F}(-\tilde{l}, \widetilde{L}, \widetilde{G}, \widetilde{H}, \omega). \tag{18}$$

This implies that in the spatial case the structure of the phase space is generally asymmetrical with respect to $\tilde{l} = 0°$ (for instance, Figures 3(b) and (d)).

In the spatial case, the collision event occurs only when the orbits of the small body and the planet interact at the ascending or descending node of the small body's orbit. This requires that ω must satisfy (Nesvorný et al. 2002)

$$\cos\omega = \pm\frac{1}{e}\left[\frac{a}{a'}(1 - e^2) - 1\right]. \tag{19}$$

Thus, there is generally no collision singularity except for specific values of ω. The collision singularity is replaced by the local maxima of the Hamiltonian as well as $S(\tilde{l})$. The existence of the local maxima and the asymmetry of the Hamiltonian lead to the appearance of the compound orbits (Figure 4).

Figure 4 shows the behavior of $S(\tilde{l})$ for a selection of reference elements same as in Figure 3. In Figures 4(b)–(d) there are two peaks S_- and S_+ situated at the left and right of $\tilde{l} = 0°$ respectively. We have $S_- > S_+$ for the asymmetrical cases (Figures 4(b) and (d)). From Figure 4 we find that: if $S_- > S_+ > S_{L_3}$ the asymmetrical H–QS orbits exist (see Figures 4(b)); if $S_{L_3} > S_-$ the T–QS-T orbits exist (Figures 4(c) and (d)); and if $S_{L_3} > S_- > S_+ > S_{L_4}$ we have the T–QS orbits (Figure 4(d)).

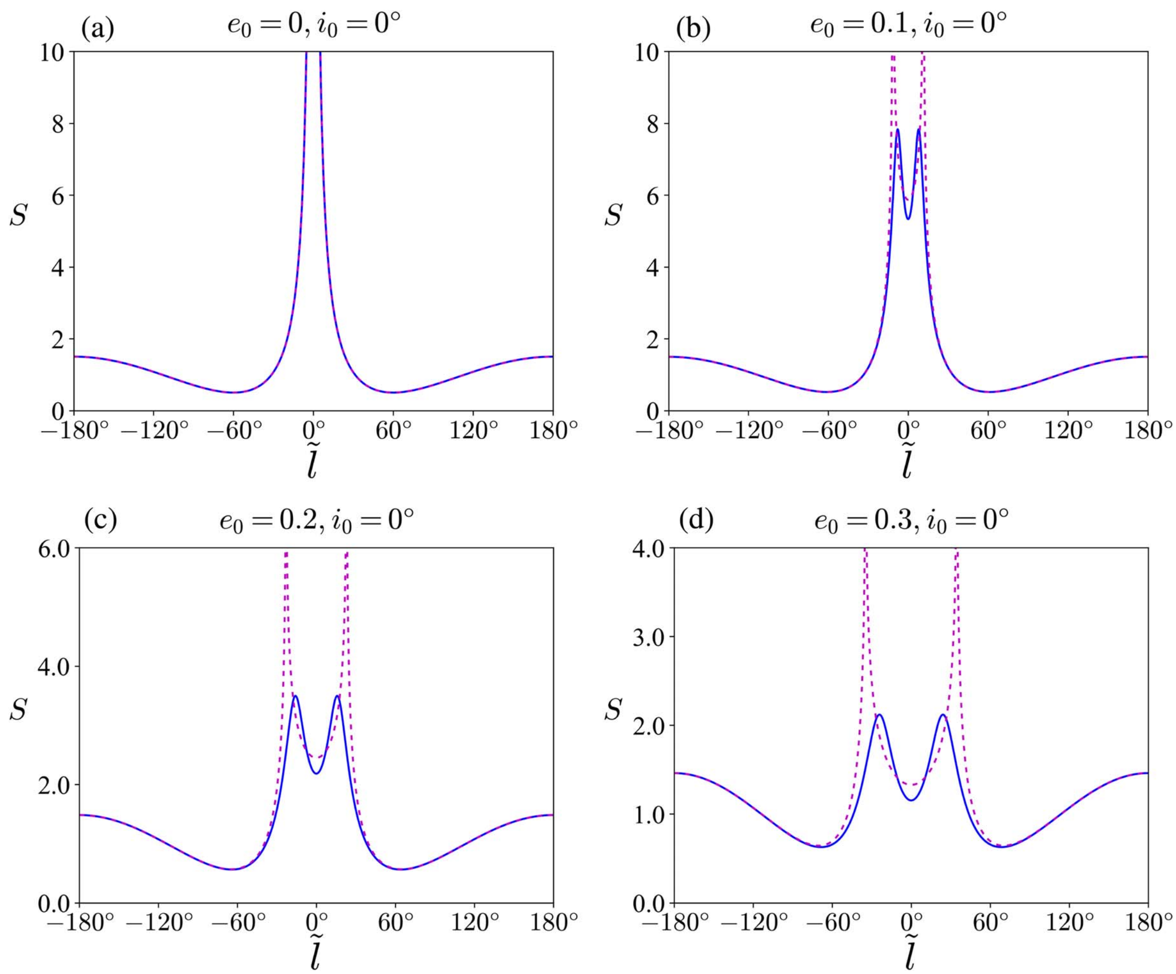

Figure 5. A comparison of the behavior of S between the analytical averaged model (solid lines) and the numerical averaged model (dashed lines) for the planar case.

4. Comparison with the Numerical Averaged Model

In this section we compare the analytical averaged model with the numerical averaged model. Note that the only difference of the two models is in the averaged disturbing function $\overline{R}$. Therefore, by comparing the behavior of S between the two models we can evaluate how the analytical averaged model agrees with the numerical averaged model.

A comparison of the behavior of S in the analytical and numerical averaged models for the planar case is shown in Figure 5. We see that the analytical averaged model is in complete agreement with the numerical averaged model for $e_0 = 0$ (Figure 5(a)). Both models give a collision singularity at $\tilde{l} = 0°$.

For $e_0 > 0$, the collision singularity has been removed from the analytical averaged model and is replaced by the local maxima, while the numerical averaged model has two singularities at both sides of $\tilde{l} = 0°$ (see Figures 5(b)–(d)). However, as illustrated in Section 3.1, both the analytical and

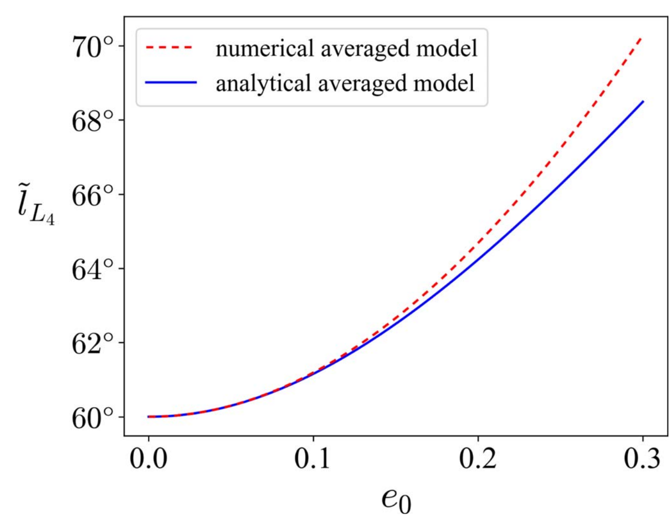

Figure 6. The location of the L_4 Lagrangian point, $\tilde{l}_{L4}$, as a function of e_0. The red line represents the result given by the numerical averaged model, and the blue line given by the analytical model.

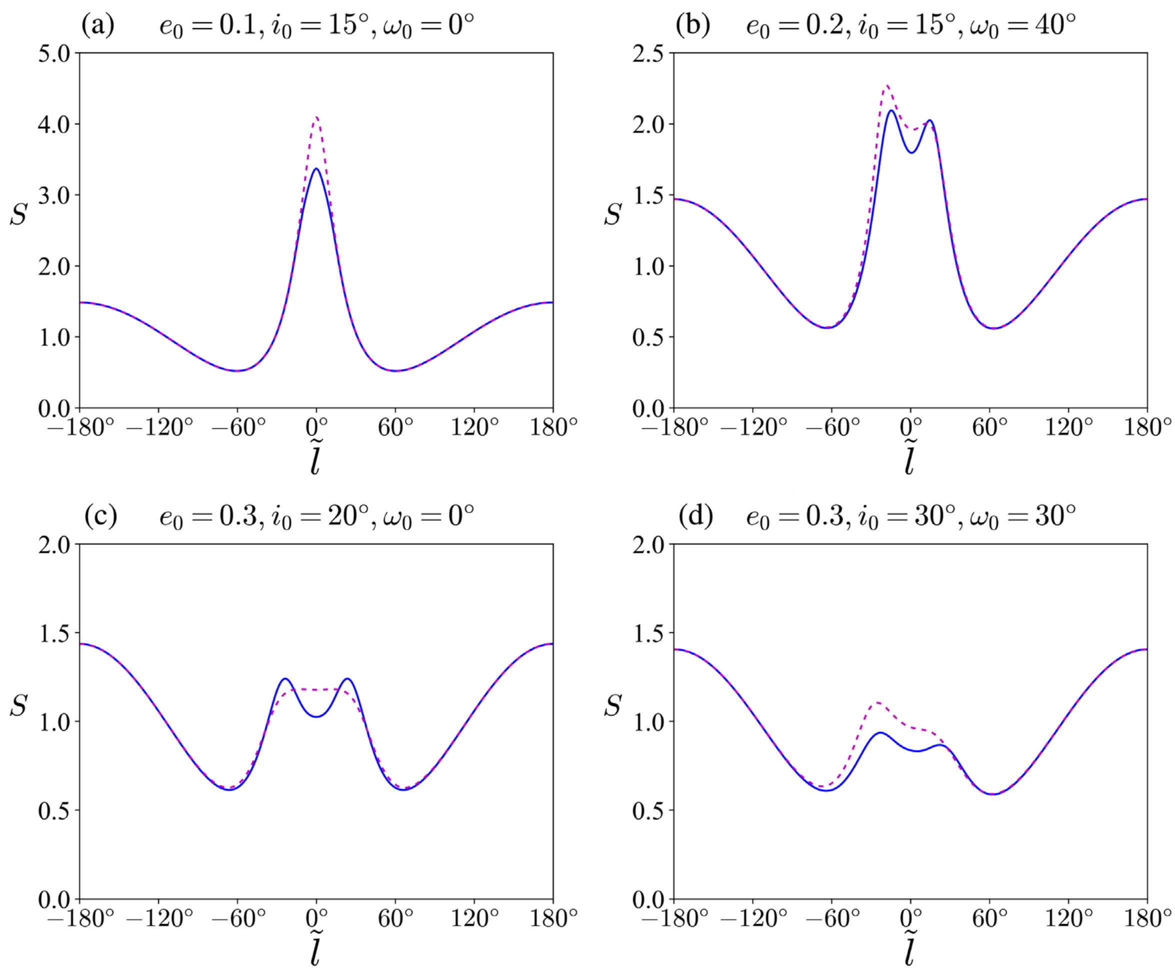

Figure 7. The same as Figure 5 but for the spatial case.

numerical averaged models are not valid in the vicinity of the collision singularity, and neither of them can reflect properly the real dynamics in that region. Thus, this inconsistency between the two models may be ignored. Except near the collision singularity, the analytical averaged model agrees with the numerical averaged model well even for $e_0 = 0.3$ (Figures 5(b)–(d)).

The minima of S define the location of the Lagrangian points L_4 and L_5. Thus, by finding the root of the equation $dS/d\tilde{l} = 0$, we can determine the displacement of the location of the Lagrangian point L_4 (or L_5) from $\tilde{l} = 60°$ (or $\tilde{l} = 300°$) for different values of e_0. The result is shown in Figure 6. We can see that the Lagrangian point L_4 drifts outward from $\tilde{l} = 60°$ with increasing e_0 for both the numerical and analytical averaged models. Importantly, for $e_0 < 0.3$ there is a quite small deviation between the analytical model and the numerical averaged model.

Figure 7 provides a comparison of the analytical averaged model with the numerical averaged model for the spatial case for a selection of reference elements, the same as that in Figure 3. It is clear from Figure 7 that for the moderate eccentricities and inclinations the behavior of S of the analytical averaged model is basically consistent with that of the numerical averaged model, although there are quantitative differences especially in the peaks S_- and S_+ and the local minimum S_0.

In the numerical averaged model, the peak S_- actually corresponds to the minimum relative distance, $\Delta_{\min}$, between the small body and the planet. $\Delta_{\min}$ is a function of a, e, i and ω. For $a = 1$, $e = 0.3$, from Equation (19) we get $\omega \approx 72.5°$ for which the collision singularity occurs. This means that as $\omega \to 72.5°$ the minimum relative distance $\Delta_{\min}$ tends to zero. Figure 8 shows that for the case of $e_0 = 0.3$, $i_0 = 30°$ there is considerable disagreement between the analytical and numerical models when ω_0 is close to the value of $72.5°$. In Figure 8, the numerical averaged model gives a very high and sharp peak S_- to the left of $\tilde{l} = 0°$ for $\omega_0 = 60°$ and $72°$, corresponding to quite small values of $\Delta_{\min}$; and yet the analytical averaged

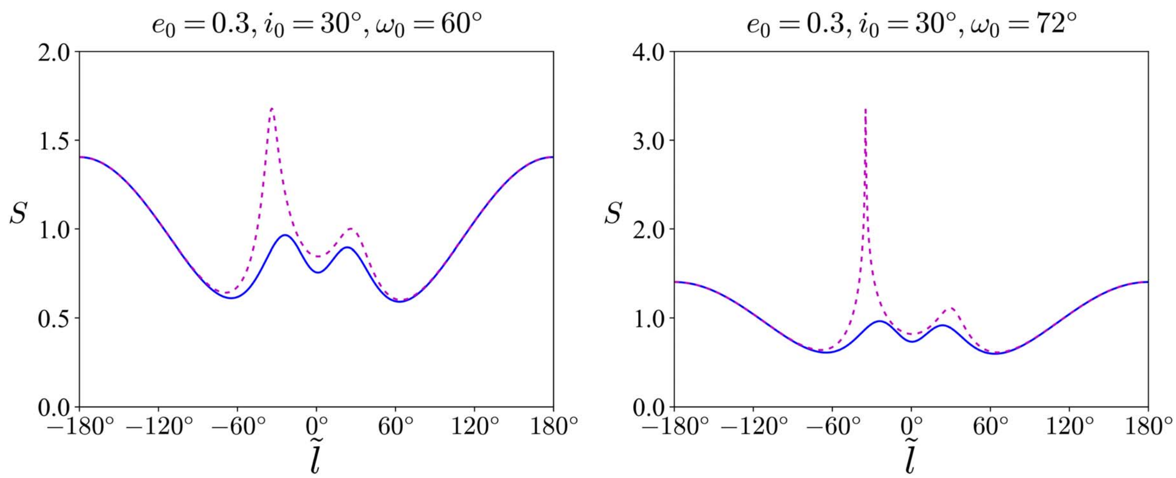

Figure 8. The behavior of S of the analytical averaged model (solid lines) and of the numerical averaged model (dashed lines) for small values of $\Delta_{\min}$.

model gives a low and soft peak S_-. This is because in the analytical averaged model the local maximum S_- has been softened as a result of the elimination of the collision singularity. The softening maximum S_- cannot reach a very large value.

From the behavior of S shown in Figure 8 we see that the analytical averaged model gives the compound T–QS-T orbits; however, due to the existence of the sharp peak S_-, there are the compound H–QS orbits instead of the T–QS-T orbits in the numerical averaged model. Consequently, the phase-space structure of the numerical averaged model is now qualitatively different from that of the analytical averaged model. This indicates that in such cases the analytical averaged model is not sufficient to describe the co-orbital dynamics especially for the compound orbits. However, from Figures 5, 7 and 8 we note that the analytical averaged model is always a good approximation to the tadpole and horseshoe motions.

5. Conclusions

In this paper we focused on the co-orbital motion in the circular restricted three-body problem, which consisted of a massless small body moving around a central star and perturbed by a planet in a circular orbit. We developed an analytical model adapted to the planar and spatial 1:1 resonance and valid in the entire con-orbital region. It takes two main steps to construct the model: first, we expanded the Hamiltonian of the circular restricted three-body problem to the second order in the eccentricity and inclination of the small body; then we averaged the result with respect to the mean anomaly of the small body and we obtained an analytical averaged Hamiltonian.

For the planar 1:1 resonance, our analytical averaged model can recover three classical types of the co-orbital motion: tadpole, horseshoe and quasi-satellite orbits. Moreover, the analytical model shows that as the eccentricity increases the quasi-satellite domain becomes larger and larger, which is consistent with the previous works. The shift of the Lagrangian points L_4 and L_5 was also observed in the analytical model. For the spatial 1:1 resonance, the analytical model reveals that the phase space structure is generally asymmetrical. There are the compound H–QS, T–QS and T–QS-T orbits which are formed by the merger of the quasi-satellite orbits with the horseshoe or tadpole orbits. The appearance of these compound orbits is due to the existence of the local maxima and the asymmetry of the Hamiltonian.

Comparison with the numerical averaged model shows that our analytical averaged model is valid even for the moderate eccentricities (∼0.3) and inclinations (∼30°). However, the analytical averaged model becomes a poor approximation to the dynamics in the vicinity of the collision singularity, for two reasons. First, the averaged method is not applicable to the motion inside the Hill region in which the timescales of the different degrees of freedom of the system are not separated well. Second, in the the analytical averaged model the local maxima of the Hamiltonian are softened as a consequence of the fact that the collision singularity is removed from the Hamiltonian. The softening maxima cannot reach a very large value when the minimum relative distance approaches zero, which would lead to the co-orbital dynamics qualitatively different from that of the numerical averaged model.

This paper may be helpful for relevant researches. For example, we can exploit the analytical model to calculate the oscillation amplitude and period of the co-orbital orbits. The averaged analytical model can be further used to study the secular stability of the co-orbital motion (especially for the tadpole and horseshoe orbits). Specifically, we can analytically study the orbital stability of the Trojan asteroids in tadpole orbits around the L_4 and L_5 Jovian Lagrangian points. We want to examine whether the number asymmetry of the L_4 and L_5 Jovian Trojans is related to the stability of the co-orbital motion at the L_4 and L_5 points. Moreover, using the analytical model we may provide a qualitative analysis of the secular stability of some recent found asteroids co-orbiting with the Earth (Borisov et al. 2023). According to the analytical Hamiltonian, we may develop a secular formalism of the circular RTBP to study the secular evolution of the eccentricity and inclination of the co-orbital objects. Furthermore, the co-orbital motion in the elliptic restricted three-body problem may also be approached analytically by using the methods presented in the paper.

Acknowledgments

We thank the anonymous referee for helpful comments and suggestions for improving this paper. The work is supported by the National Natural Science Foundation of China (NSFC) (grant No. 11973010).

Appendix
Analytical Expression for the Averaged Hamiltonian

The averaged Hamiltonian is given by

$$\overline{F} = -\frac{\mu^2}{2\tilde{L}^2} - n'\tilde{L} - Gm'\left[\overline{\left(\frac{1}{\Delta}\right)} - \frac{\overline{r\cos\psi}}{a'^{\,2}}\right], \tag{A1}$$

with

$$\begin{aligned}\overline{\left(\frac{1}{\Delta}\right)} &= \frac{1}{2\pi}\int_0^{2\pi}\frac{1}{\Delta}\,\mathrm{d}M\\ \overline{r\cos\psi} &= \frac{1}{2\pi}\int_0^{2\pi} r\cos\psi\,\mathrm{d}M.\end{aligned} \tag{A2}$$

To obtain an analytical expression for the averaged Hamiltonian, the first and most crucial step is to expand the direct term of the disturbing function, Δ^{-1}, written as

$$\begin{aligned}\frac{1}{\Delta} = \Big[r^2 + a'^2 - 2ra'\Big(&\cos^2\frac{i}{2}\cos(\theta - M')\\ &+\sin^2\frac{i}{2}\cos(\theta + M' - 2\Omega)\Big)\Big]^{-1/2}.\end{aligned} \tag{A3}$$

Since we focus on the prograde orbits of the small body in this paper, here $\sin^2(i/2)$ is a small quantity. Therefore, Δ^{-1} can be expanded in a Taylor series in $\sin^2(i/2)$. We have

$$\begin{aligned}\frac{1}{\Delta} &= \frac{1}{\Delta_0} + \frac{ra'\sin^2(i/2)\cos(\theta + M' - 2\Omega)}{\Delta_0^3}\\ &+ \mathcal{O}\left(\sin^4\frac{i}{2}\right),\end{aligned} \tag{A4}$$

where

$$\Delta_0 = \left(r^2 + a'^{\,2} - 2ra'\cos^2\frac{i}{2}\cos(\theta - M')\right)^{1/2}. \tag{A5}$$

One can easily obtain the elliptic expansions to the second order in e for r^2, $r\cos(\theta - M')$ and $r\cos(\theta + M' - 2\Omega)$. They are

$$r^2 = a^2\left[\left(1 + \frac{3}{2}e^2\right) - 2e\cos M - \frac{1}{2}e^2\cos 2M\right] + \mathcal{O}(e^3), \tag{A6}$$

$$\begin{aligned}r\cos(\theta - M') = a\Big[&\frac{1}{8}e^2\cos(\tilde{l} - 2M) - \frac{3}{2}e\cos(\tilde{l} - M)\\ &+\left(1 - \frac{1}{2}e^2\right)\cos\tilde{l}\\ &+\frac{1}{2}e\cos(\tilde{l} + M) + \frac{3}{8}e^2\cos(\tilde{l} + 2M)\Big]\\ &+\mathcal{O}(e^3),\end{aligned} \tag{A7}$$

$$\begin{aligned}r\cos(\theta + M' - 2\Omega) = a\Big[&\frac{1}{8}e^2\cos(\tilde{l} - 2\omega)\\ &-\frac{3}{2}e\cos(\tilde{l} - 2\omega - M)\\ &+\left(1 - \frac{1}{2}e^2\right)\cos(\tilde{l} - 2\omega - 2M)\\ &+\frac{1}{2}e\cos(\tilde{l} - 2\omega - 3M)\\ &+\frac{3}{8}e^2\cos(\tilde{l} - 2\omega - 4M)\Big] + \mathcal{O}(e^3).\end{aligned} \tag{A8}$$

By making use of the expansions Equation (A6) and Equation (A7), Δ_0^2 can be split into

$$\Delta_0^2 = \Delta_{00}^2 - (Ae + Be^2), \tag{A9}$$

where

$$\begin{aligned}\Delta_{00}^2 &= a^2\left(1 + \frac{3}{2}e^2\right) + a'^{\,2}\\ &- 2aa'\left(1 - \frac{1}{2}e^2\right)\cos^2\frac{i}{2}\cos\tilde{l},\end{aligned} \tag{A10}$$

$$\begin{aligned}A = 2a^2\cos 2M - aa'\cos^2\frac{i}{2}[&3\cos(\tilde{l} - M)\\ &-\cos(\tilde{l} + M)],\end{aligned} \tag{A11}$$

$$\begin{aligned}B &= \frac{1}{2}a^2\cos 2M + aa'\cos^2\frac{i}{2}\\ &\times\left[\frac{1}{4}\cos(\tilde{l} - 2M) + \frac{3}{4}\cos(\tilde{l} + 2M)\right].\end{aligned} \tag{A12}$$

Δ_{00}^2 is of order $\mathcal{O}(1)$. From Equation (A9), we have

$$\frac{1}{\Delta_0} = \frac{1}{\Delta_{00}} + \frac{1}{2}\frac{(Ae + Be^2)}{\Delta_{00}^3} + \frac{3}{8}\frac{A^2e^2}{\Delta_{00}^5} + \mathcal{O}(e^3), \tag{A13}$$

$$\frac{1}{\Delta_0^3} = \frac{1}{\Delta_{00}^3} + \frac{3}{2}\frac{(Ae + Be^2)}{\Delta_{00}^5} + \frac{15}{8}\frac{A^2e^2}{\Delta_{00}^7} + \mathcal{O}(e^3). \tag{A14}$$

Substituting Equations (A13) and (A14) into Equation (A4) and averaging over the mean anomaly M (and keeping terms up to order e^2), we obtain

$$\overline{\left(\frac{1}{\Delta}\right)} = \overline{\left(\frac{1}{\Delta_0}\right)} + e^2 \sin^2\frac{i}{2}\,\frac{aa'}{\Delta_{00}^3} \times \left\{\left[\frac{1}{8} - \frac{15}{8}\frac{a^2}{\Delta_{00}^2} + \frac{15}{8}\frac{a^4}{\Delta_{00}^4} - \frac{45}{16}\frac{a^2a'^2}{\Delta_{00}^4}\cos^4\frac{i}{2}\right]\cos(\tilde{l} - 2\omega) + \left[\frac{57}{16}\frac{aa'}{\Delta_{00}^2} - \frac{45}{8}\frac{a^3a'}{\Delta_{00}^4}\right]\cos^2\frac{i}{2}\cos 2\omega + \left[-\frac{9}{16}\frac{aa'}{\Delta_{00}^2} + \frac{15}{8}\frac{a^3a'}{\Delta_{00}^4}\right]\cos^2\frac{i}{2}\cos(2\tilde{l} - 2\omega) + \frac{135}{32}\frac{a^2a'^2}{\Delta_{00}^4}\cos^4\frac{i}{2}\cos(\tilde{l} + 2\omega) + \frac{15}{32}\frac{a^2a'^2}{\Delta_{00}^4}\cos^4\frac{i}{2}\cos(3\tilde{l} - 2\omega)\right\}, \quad \text{(A15)}$$

with

$$\overline{\left(\frac{1}{\Delta_0}\right)} = \frac{1}{\Delta_{00}} + \frac{3}{8}\frac{\Delta_{01}^2}{\Delta_{00}^5}, \quad \text{(A16)}$$

and

$$\Delta_{01}^2 = e^2\left(2a^4 + 5a^2a'^2\cos^4\frac{i}{2}\right) - 4e^2a^3a'\cos^2\frac{i}{2}\cos\tilde{l} - 3e^2a^2a'^2\cos^4\frac{i}{2}\cos 2\tilde{l}. \quad \text{(A17)}$$

$\overline{(1/\Delta_0)}$ can be written in the form

$$\overline{\left(\frac{1}{\Delta_0}\right)} = \frac{1}{2}\left[\frac{1}{\sqrt{\Delta_{00}^2 - \Delta_{01}}} + \frac{1}{\sqrt{\Delta_{00}^2 + \Delta_{01}}}\right], \quad \text{(A18)}$$

which provides a better approximation for the 1:1 resonance when the small body approaches the planet closely. From Equations Equation (A7) and Equation (A8) it is easy to find

$$\overline{r\cos\psi} = a\left[\cos^2\frac{i}{2}\left(1 - \frac{1}{2}e^2\right)\cos\tilde{l} + \frac{1}{8}e^2\sin^2\frac{i}{2}\cos(\tilde{l} - 2\omega)\right]. \quad \text{(A19)}$$

References

Beaugé, C., & Roig, F. 2001, Icarus, 153, 391
Borisov, G. B., Christou, A. A., & Apostolovska, G. 2023, Planet. Space Sci., 225, 105619
Brasser, R., Innanen, K. A., Connors, M., et al. 2004, Icarus, 171, 102
Christou, A. A. 2000, Icarus, 144, 1
de la Fuente Marcos, C., & de la Fuente Marcos, R. 2014, MNRAS, 445, 2985
de la Fuente Marcos, C., & de la Fuente Marcos, R. 2016, MNRAS, 462, 3344
Dermott, S. F., & Murray, C. D. 1981a, Icarus, 48, 1
Dermott, S. F., & Murray, C. D. 1981b, Icarus, 48, 12
Gallardo, T. 2006, Icarus, 184, 29
Gascheau, M. 1843, CR, 16, 393
Giuppone, C. A., Beaugé, C., Michtchenko, T. A., & Ferraz-Mello, S. 2010, MNRAS, 407, 390
Giuppone, C. A., & Leiva, A. M. 2016, MNRAS, 460, 966
Greenstreet, S., Gladman, B., & Ngo, H. 2020, AJ, 160, 144
Kaplan, M., & Cengiz, S. 2020, MNRAS, 496, 4420
Leleu, A., Robutel, P., & Correia, A. 2018, CeMDA, 130, 1
Mikkola, S., Brasser, R., Wiegert, P., & Innanen, K. 2004, MNRAS, 351, L63
Morais, M. H. M. 1999, A&A, 350, 318
Morais, M. H. M. 2001, A&A, 369, 677
Namouni, F. 1999, Icarus, 137, 293
Namouni, F., Christou, A. A., & Murray, C. D. 1999, PhRvL, 83, 2506
Namouni, F., & Murray, C. D. 2000, CeMDA, 76, 131
Nesvorný, D., Thomas, F., Ferraz-Mello, S., & Morbidelli, A. 2002, CeMDA, 82, 323
Pousse, A., Robutel, P., & Vienne, A. 2017, CeMDA, 128, 383
Qi, Y., & de Ruiter, A. 2020, MNRAS, 494, 4695
Robutel, P., Niederman, L., & Pousse, A. 2016, JCoAM, 35, 675
Robutel, P., & Pousse, A. 2013, CeMDA, 117, 17
Schubart, J. 1964, SAO Special Report, 149
Sidorenko, V. V., Neishtadt, A. I., Artemyev, A. V., & Zelenyi, L. M. 2014, CeMDA, 120, 131
Synnott, S. P., Peters, C. F., Smith, B. A., & Morabito, L. A. 1981, Sci, 212, 191
Wajer, P. 2009, Icarus, 200, 147
Wiegert, P. A., Innanen, K. A., & Mikkola, S. 1998, AJ, 115, 2604
Wisdom, J. 1985, Icarus, 63, 272
Yoder, C. F., Colombo, G., Synnott, S. P., & Yoder, K. A. 1983, Icarus, 53, 431